Primary instability of a shear-thinning film flow down an incline: experimental study

M. H. Allouche[1,2], **V. Botton**[1,2], **S. Millet**[1], **D. Henry**[1], **S. Dagois-Bohy**[1,†], **B. Güzel**[1,3] and **H. Ben Hadid**[1]

[1]Laboratoire de Mécanique des Fluides et d'Acoustique, CNRS/Université de Lyon, École Centrale de Lyon/Université Lyon 1/INSA de Lyon, ECL, 36 avenue Guy de Collongue, 69134 Ecully CEDEX, France

[2]INSA Euro-Méditerranée, Université Euro-Méditerranéenne de Fès, Route de Meknès, BP51, Fez, Morocco

[3]Yildiz Technical University, Department of Naval Architecture and Marine Engineering, Marine Machinery, 34349 Yildiz, Istanbul, Turkey

The main objective of this work is to study experimentally the primary instability of non-Newtonian film flows down an inclined plane. We focus on low-concentration shear-thinning aqueous solutions obeying the Carreau law. The experimental study essentially consists of measuring wavelengths in marginal conditions, which yields the primary stability threshold for a given slope. The experimental results for neutral curves presented in the (Re, f_c) and (Re, k) planes (where f_c is the driving frequency, k is the wavenumber and Re is the Reynolds number) are in good agreement with the numerical results obtained by a resolution of the generalized Orr–Sommerfeld equation. The long-wave asymptotic extension of our results is consistent with former theoretical predictions of the critical Reynolds number. This is the first experimental evidence of the destabilizing effect of the shear-thinning behaviour in comparison with the Newtonian case: the critical Reynolds number is smaller, and the ratio between the critical wave celerity and the flow velocity at the free surface is larger.

1. Introduction

Shallow-water flows on a slope featuring a free surface often present an unstable motion, characterized by various types of surface waves. These waves may be complex, depending on inertia, inclination or fluid properties. If the waves that are triggered in such flows are initially quasiplane with large wavelength, farther

† Email address for correspondence: simon.dagois-bohy@univ-lyon1.fr

downstream they grow in amplitude and quickly evolve towards a nonlinear regime. In this paper, an experimental study is performed to investigate the stability of such films when the fluid is shear-thinning, a relevant configuration for many geophysical flows such as debris flows or mud surge waves.

In the case of Newtonian fluids, the onset of such waves is well understood since the early linear theoretical studies of Benjamin (1957) and Yih (1963), who showed that the critical Reynolds number for the onset of the instabilities only depends on the slope angle, and is proportional to its cotangent. The same value is obtained with shallow-water or Orr–Sommerfeld approaches, as long as the long-wave hypothesis is used. This cotangent dependence was later confirmed experimentally by Liu, Paul & Gollub (1993).

Smith (1990) proposed a phenomenological approach in order to understand the physical mechanisms for the long-wave instability in Newtonian thin liquid films. (i) He showed that the disturbance of the free surface is the trigger point of the shear-induced instability, which is consistent, in shallow-water models, with the existence of a kinematic wave that is exclusively governed by the conservation of mass (Kalliadasis *et al.* 2011; Whitham 2011). (ii) He investigated the effect of the stabilizing and destabilizing terms in the growth phase of the instability, which, at the leading orders in the long-wave expansion theory, correspond to the responses of the film to the variation in momentum through dynamic waves (Kalliadasis *et al.* 2011). (iii) He wrote the mass balance equation in the wave framework and showed that, at the linear threshold, the waves travel two times faster than the flow velocity at the free surface, this latter point being a key ingredient in this inertia-driven instability.

In the literature, most experimental studies on waves down an incline are based on a Newtonian fluid model (Liu *et al.* 1993; Vlachogiannis *et al.* 2010; Georgantaki *et al.* 2011). However, in many engineering applications (coating processes in paint, paper, food, plastic, etc. industries) or geophysical phenomena (glaciers, mud and debris flows), the liquids involved present more complex rheological behaviours (Benchabane & Bekkour 2008; Chambon, Ghemmour & Laigle 2009; Jouvet *et al.* 2011). In particular, the viscoplastic rheology was shown to describe quite well the global behaviour of the materials involved in debris flows (Huang & Garcia 1998; Chambon *et al.* 2009). Most viscoplastic liquids are not ideal Bingham liquids and have shear-thinning properties in addition to the yield stress. In this study, we chose to focus on purely shear-thinning fluids and leave the yield stress out, for the sake of simplicity. This should be seen as a first step towards understanding the physics of complex fluids. Moreover, this simplified rheology could already be sufficient to describe some real geological materials (Jeong 2010).

Several models are available to describe the rheology of shear-thinning fluids, among which is the power-law model. Under the shallow-water approximation, the stability of a film of a power-law fluid flowing down an inclined plane has been studied theoretically by several authors (Ng & Mei 1994; Dandapat & Mukhopadhyay 2001; Amaouche, Djema & Bourdache 2009; Fernández-Nieto, Noble & Vila 2010). However, this rheology yields an infinite viscosity at zero shear rate (i.e. at the surface), which demands a careful handling in theoretical computation of the critical Reynolds number (Noble & Vila 2013). Moreover, this rheology is sometimes not physically accurate, for example in the case of polymer solutions and melts, whose viscosities always remain finite.

To solve this issue, Ruyer-Quil, Chakraborty & Dandapat (2012) recently modified the power-law model by introducing a Newtonian plateau at low values of the shear rate, and they provided asymptotic expressions for the critical Reynolds number under the long-wave expansion.

It is possible, however, to describe such behaviour without introducing discontinuities by using a Carreau law (see § 2), and this approach is preferred by many authors, notably in the polymer and coating communities (Weinstein 1990; Rodd, Dunstan & Boger 2000; Escudier *et al.* 2001; Benchabane & Bekkour 2008). Rousset *et al.* (2007) and Millet *et al.* (2008) numerically studied flows of Carreau fluids down an incline. They investigated the influence of the Carreau law parameters on the modification of the stability threshold, using temporal stability analysis based on the Orr–Sommerfeld equation. Following the same approach as Smith (1990), they found that (i) the critical Reynolds number is lower than that for a Newtonian fluid having a viscosity equal to the zero-shear-rate viscosity of the Carreau fluid and (ii) the critical wave celerity, normalized by the surface velocity, is larger. They concluded that shear-thinning rheology has a destabilizing effect.

In contrast, on the experimental side, the literature is less abundant. The first experimental visualization record of surface waves in Newtonian falling films was the paper by Kapitza & Kapitza (1949). However, it was not until the work of Liu *et al.* (1993) that the theoretical predictions of Benjamin (1957) and Yih (1963) were confirmed experimentally. In particular, Liu *et al.* (1993) confirmed the convective nature of this instability, which has the practical consequence of making it extremely sensitive to external noise.

There is very little work on flows of non-Newtonian fluids down a slope, apart from three notable exceptions. First, Coussot (1994) investigated the stability of mud flows down an incline. Later, Forterre & Pouliquen (2003) adapted the set-up of Liu *et al.* (1993) to investigate this instability in the different, but related, context of granular flows. Finally, Chambon, Ghemmour & Naaim (2014) recently developed an original experimental configuration in which a viscoplastic surge is stationary in the laboratory frame.

In this paper, we present an experimental study on the stability of gravity-driven film flows when the fluid is shear-thinning. In the next section, we will describe our experimental set-up, which is similar to the one used by Liu *et al.* (1993). We will then present results obtained with Newtonian fluid and compare them favourably with the literature. Finally, we will present our results obtained for shear-thinning fluids, and we will compare them with models and numerical simulations.

2. Experimental set-up

2.1. *Description*

The experiments were carried out in an inclined channel of length 2 m and width $W_{ch} = 46$ cm, in which a flowing film was perturbed upstream, and the perturbation was recorded further downstream. The channel ended in a reservoir, and with a PCM EcoMoineau^{TM} progressing cavity pump, the fluid was pumped up to a manifold at the entrance of the channel (filters were used to tranquilize the flow). The flow rate q was measured with a Rosemount electromagnetic flow meter. To allow optical measurements (see below), the channel base was chosen transparent (glass).

The inclination angle of the channel, ϕ, was adjustable thanks to a telescopic motorized leg holding the end of the channel, from $0°$ up to $15°$ with a precision of $0.5°$. A sketch of the set-up is shown in figure 1.

We chose to study primary waves in the linear regime, for which the disturbances are almost two-dimensional and sinusoidal, and their amplitude is as small as possible. To impose such perturbations with controlled frequency f and amplitude A, we used a vibration device (B&K 4809) linked to a blade plunged in the upstream manifold.
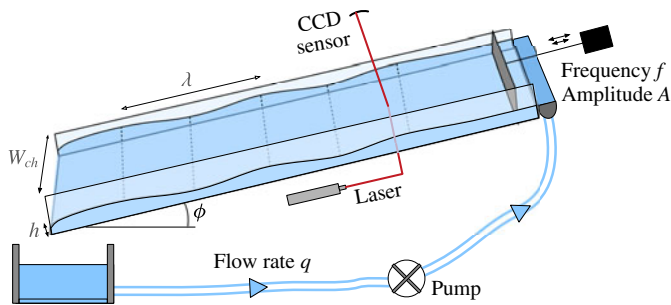
FIGURE 1. Sketch of the experimental apparatus.

This system allowed us to produce quasiplane waves with an amplitude A smaller than one millimetre, and a wavelength λ of a few centimetres. The perturbations are sinusoidal close to the channel entrance, but as they grow downstream, they evolve into complex solitary waves. This nonlinear regime has been the subject of many other studies (see, e.g., Denner *et al.* 2016), but it is not in the scope of the present study. Instead, we focused on the onset of the instability, and all our measurements were made close to the entrance manifold, i.e. still in the linear regime.

2.2. *Detection methods*

We used two detection methods to monitor the propagation of the perturbation, a local one (point measurement) and a global one (surface measurement).

The local method was the same technique as used by Liu *et al.* (1993): a laser beam was shot perpendicularly through the channel and was deflected by the liquid–air interface. A position sensitive device (PSD) recorded the laser beam position, from which the local slope of the free surface, $\mathrm{d}h/\mathrm{d}x$, was inferred. To prevent the signals from being affected by non-planar effects (e.g. induced by the walls), we always made sure that we used this method at the centreline of the channel. We repeated this measurement at regularly spaced positions, and we measured the signal amplitude (by synchronous demodulation) and the phase shift with a reference signal (the vibration device generating the waves). From these measurements we were able to extract the amplitude variation and the wavelength of the surface waves.

We also used free-surface synthetic schlieren (FS-SS) to test for wave planarity. This technique, proposed by Moisy, Rabaud & Salsac (2009), allows an instant global measurement of the free-surface slope. A pattern of computer-generated random dots is placed under the channel, approximately 70 cm below the free surface. A CCD camera (resolution 1280×1024) located 170 cm above it records its image. When the liquid surface is modified by the perturbation, the image is different from the original pattern, and by tracking the apparent displacement of the dots with standard PIV software (DaVis, LaVision), we are able to reconstruct the free-surface slope over a 40 cm long domain, located roughly 40 cm from the entrance manifold. The decay rate α and wavenumber k are then determined by fitting the surface slope measurements to the analytical expression

$$\frac{\mathrm{d}h}{\mathrm{d}x} \propto \mathrm{e}^{-\alpha x} \cos(kx - 2\pi f t). \qquad (2.1)$$
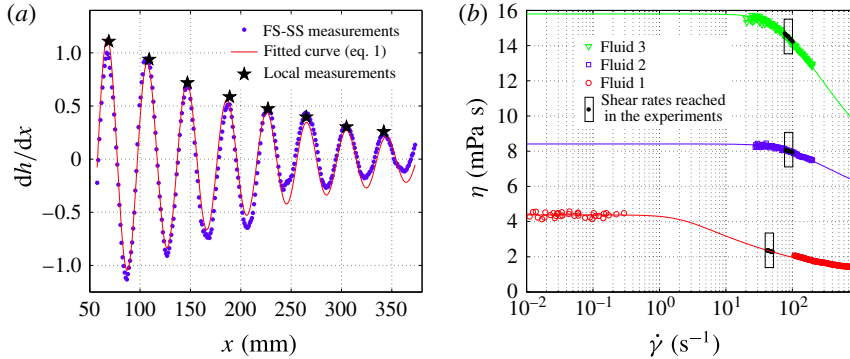
FIGURE 2. (*a*) Normalized surface slope versus position for the FS-SS method at a given time, and for the corresponding local measurements (60 % vol. water–glycerol solution, $\phi = 1°$, $Re = 23$, $f = 15$ Hz). (*b*) Rheological law for fluids 1, 2 and 3 (from bottom to top). Solid lines: fit with a Carreau law. Black points and rectangles: shear rates in the experiments (see § 4).

Figure 2(*a*) compares the results obtained with the two techniques. The good agreement with (2.1) gives us confidence in both techniques. In practice, we mostly used the local detection, first because the linear regime is located near the channel entrance, hardly accessible to the FS-SS technique, and second because it is much simpler to use.

2.3. *Fluids*

A 60 % vol. water–glycerol mixture was used for its Newtonian properties, whereas mixed solutions of both carboxymethylcellulose (CMC, E466) and xanthan gum (E415) were used as shear-thinning fluids.

The rheology of the non-Newtonian fluids is well described by a four-parameter Carreau inelastic model,

$$\frac{\eta - \eta_\infty}{\eta_0 - \eta_\infty} = \left[1 + \left(\frac{\dot{\gamma}}{\dot{\gamma}_c} \right)^2 \right]^{(n-1)/2}, \tag{2.2}$$

where η_0 and η_∞ are the limit Newtonian viscosities at zero and infinite shear rate respectively, $\dot{\gamma}_c$ is the critical shear rate separating the Newtonian and shear-thinning behaviours, n is the power-law index, η is the local viscosity and $\dot{\gamma}$ is the local shear rate.

A Rheomat™ RM115-A Couette rheometer (Lamy Rheology, 10 mN m torque) was used for the main flow curve determination. However, because most commercial rheometers are torque-sensitive, it is very difficult to precisely determine the zero-shear-rate viscosity, yet this is crucial for the characterization of flows featuring a free surface. We then implemented an electro-capillary technique to measure, when possible, the viscosity and surface tension of the fluids at values of the shear rate as small as 10^{-3} s^{-1}. This technique and the measurements are fully described in Allouche *et al.* (2015). The rheological parameters for the Carreau law and physical properties such as the density ρ and the surface tension σ of the three shear-thinning fluids used are displayed in table 1 and their rheograms are plotted in figure 2(*b*).

Shear-thinning fluids	η_0 (mPa s)	η_∞ (mPa s)	n	$\dot{\gamma}_c$ (s^{-1})	ρ (kg m^{-3})	σ (mN m^{-1})
1	4.43	0.05	0.79	2.23	981	48
2	8.41	0	0.88	77.80	993	45
3	15.80	0	0.80	74.10	1004	—
Newtonian fluid	11.7	—	—	—	1150	68.5

TABLE 1. The mechanical properties of the fluids used in the present study: Carreau parameters, density and surface tension. Newtonian values were obtained from Takamura, Fischer & Morrow (2012).

Based on this measured zero-shear-rate viscosity, we were able to define a Reynolds number for each experiment as $Re = \rho q / W_{ch} \eta_0$ (Rousset *et al.* 2007).

The first fluid used in this study was a xanthan gum solution at 0.008 wt%, whose rheology had been characterized in Allouche *et al.* (2015) (fluid 1 in table 1). This fluid exhibits a strong shear-thinning behaviour because its critical shear rate, $\dot{\gamma}_c$, is low. For this fluid, $\dot{\gamma}_c$ was reached even at very small inclination angles in our set-up. On the contrary, the shear-thinning behaviour in CMC solutions occurs later, at higher shear rates than we could reach in our set-up. We then decided to mix CMC and xanthan gum in different proportions to obtain moderate shear-thinning fluids.

3. Experimental test with a Newtonian fluid

In this section, we present the results obtained with a Newtonian fluid. The goal here is to compare these results with well-established results from the literature, in order to evaluate the accuracy and limits of our set-up. The measurement of the linear stability thresholds consisted of the following steps. At fixed slope ϕ, flow rate q and frequency f, we measured the wavenumber k and the decay rate α (figure 2(*a*) and (2.1)). We then repeated the measurement for different frequencies (keeping q constant) to identify the cutoff frequency f_c where the waves neither amplify nor attenuate ($\alpha = 0$), i.e. the marginal conditions. We repeated the procedure for different flow rates (i.e. different Re), keeping ϕ constant.

Figure 3(*a*) shows the obtained $f_c(Re)$ at $\phi = 3.2°$. Like Liu *et al.* (1993), we find that the cutoff frequency varies as follows:

$$f_c \propto \left(Re - Re_c^{exp} \right)^{1/2} . \tag{3.1}$$

From this, we could extract the critical Reynolds number, i.e. at zero frequency, by fitting (3.1) to our data. Finally, we repeated this procedure at different inclination angles, and we obtained the variation of Re_c^{exp} with ϕ.

It should be noted that measurements at low frequencies are very difficult: the perturbation becomes nonlinear over a distance shorter than the wavelength and generates parasitic waves (Argyriadi, Serifi & Bontozoglou 2004). Moreover, the experiment is very sensitive to external vibrations, in particular the pump rotation speed. In practice, no measurement could be made below $f \sim 2$ Hz.

We can now compare our experimental stability thresholds, shown in figure 3(*b*), with the theoretical curve of Yih (1963), given by
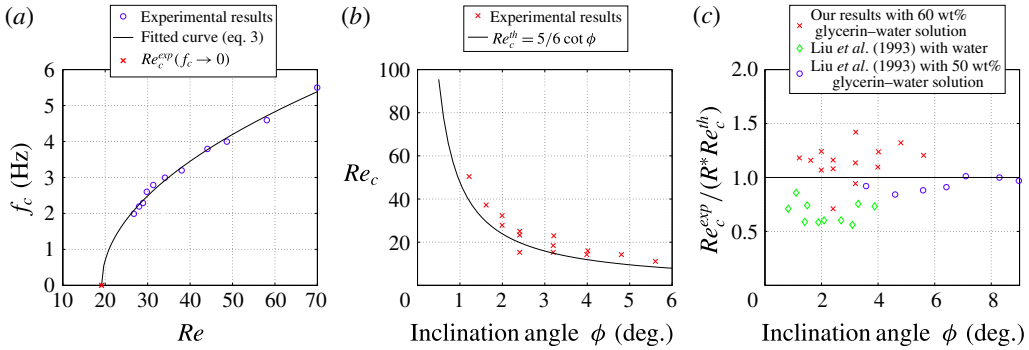
$$Re_c^{th} = \tfrac{5}{6} \cot \phi. \tag{3.2}$$

FIGURE 3. (*a*) Neutral curve in the (Re, f_c) plane for a Newtonian water–glycerol solution at $\phi = 3.2°$. (*b*) Critical Reynolds number Re_c as a function of the inclination angle. The crosses represent the experimental results Re_c^{exp} for water–glycerol solutions and the solid line corresponds to the theoretical prediction Re_c^{th} for an infinite channel (Yih 1963) (see (3.2)). (*c*) The ratio $Re_c^{exp}/(R^* Re_c^{th})$ as a function of ϕ, where R^* is the correction factor of Georgantaki *et al.* (2011).

We find that our results are in good agreement with the theory, although there is a systematic shift of a few units above the theoretical curve. We interpret this shift as an effect of the finite width. Indeed, equation (3.2) is obtained for the case of Newtonian film flows of infinite width (Yih 1963). Vlachogiannis *et al.* (2010) experimentally showed that the finite width of experimental channels stabilizes the liquid film and increases the critical Reynolds number, which is consistent with what we see in figure 3(*b*).

To further investigate the stabilizing effect of the channel width on our results, we follow the analysis by Georgantaki *et al.* (2011). They quantified the deviation from the theory $R^* = Re_c^{exp}/Re_c^{th}$, which they found to be governed by surface tension effects, and depend only on the Kapitsa number $Ka = l_c^2/l_v^2 = \sigma \rho^{1/3}/g^{1/3}\eta^{4/3}$ (where g is the gravitational acceleration, l_c is the capillary length and l_v is the viscous length). At large Ka, this deviation reaches a plateau that scales as $R_m^* \sim l_c/W_{ch}$, and at small Ka, R^* varies in first approximation as $R^* = 1 + (Ka/2000)(R_m^* - 1)$. We use this expression to evaluate the deviation from theory, with $R_m^* = 1.6$ and $Ka = 127$, yielding a correction factor of $R^* = 1.04$. Figure 3(*c*) shows the ratio $Re_c^{exp}/(R^* Re_c^{th})$ as a function of the inclination angle for both our data (crosses) and the data of Liu *et al.* (1993) (diamonds). We see that the ratio does not seem to vary with ϕ, as expected from Georgantaki *et al.* (2011). That being said, their correction is not sufficient to fully capture the deviation from the theory, both in our case and in the case of Liu *et al.* (1993). This observed discrepancy could be due to the parameters we used in our experiments. These parameters (large W_{ch}, higher viscosity and low Ka) are precisely in the range where R^* is the hardest to evaluate. In fact, the data of Georgantaki *et al.* (2011) are scarce in this range, and the linear fit we used to evaluate R^* could be wrong. A possible cause could be that at high viscosity, the capillary effects might not be the dominant stabilizing mechanism anymore. In the end, we conclude that a systematic stabilizing effect of the channel width is very likely, and we will keep it in mind when dealing with the shear-thinning fluids. However, this effect is small enough so that our experiment is able to capture the correct instability behaviour of the fluids, as seen in figures 3(*c*) and 4(*a*).
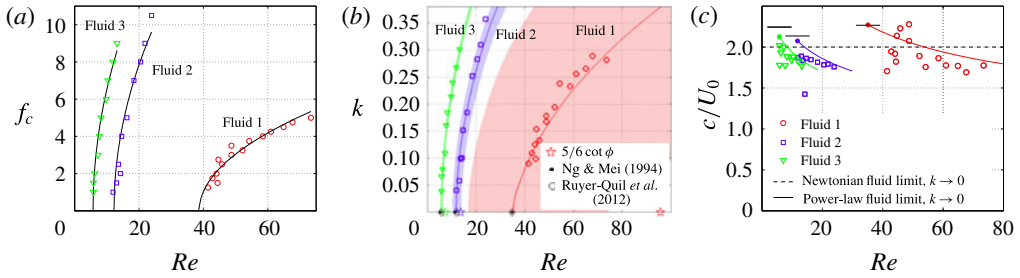
FIGURE 4. (*a*) Neutral curve in the (Re, f_c) plane for the shear-thinning fluids. Solid line: fit from (3.1). (*b*) Neutral curves in the (Re, k) plane. Solid lines: numerically obtained neutral curves for the fluids (for fluid 3, σ was set to minimize the error in the neutral curve). Coloured areas: range of numerical results corresponding to the $\Delta\phi = 0.5°$ uncertainty (except for fluid 1, where $\phi \in [0.25°, 1°]$). (*c*) Wave celerity c to surface velocity U_0 ratio as a function of Re. Coloured solid lines: numerically obtained wave celerity. The critical threshold values are reached numerically for $k \to 0$ (solid circles). Dashed line: Newtonian limit $c/U_0 = 2$. Solid lines: power-law fluid limit $c/U_0 = 1 + 1/n$.

4. Primary instability in the shear-thinning case

Before presenting the experimental stability measurements for shear-thinning fluids, we dedicate a few words to the numerical resolution of the Orr–Sommerfeld equation with which they will be compared. In the study of Rousset *et al.* (2007), a steady uniform flow is considered (flow rate q, channel width W_{ch}, inclination angle ϕ), and the linear stability equations are derived. These equations are set in dimensionless form using the characteristic scalings one would find for a Newtonian fluid of viscosity η_0 (the zero-shear viscosity of the Carreau fluid): a length scale $d_s = (\eta_0 q/\rho g W_{ch} \sin\phi)^{1/3}$, a velocity scale $v_s = (q/W_{ch}d_s)$ and a shear-rate scale $\dot{\gamma}_s = d_s/v_s$. In particular, the dimensionless Carreau law is expressed as

$$\frac{\eta}{\eta_0} = I + (1 - I)\left[1 + \left(L\dot{\Gamma}\right)^2\right]^{(n-1)/2},\qquad(4.1)$$

with $I = \eta_\infty/\eta_0$, $L = q/W_{ch}\dot{\gamma}_c d_s^2$ and $\dot{\Gamma} = \dot{\gamma}W_{ch}d_s^2/q$. Then, the perturbation growth rates are numerically calculated, which eventually gives the neutral curve and the critical Reynolds number. We want to emphasize that the parameter L has an important impact on the numerical results: when L is too large, the numerical solution becomes difficult, whereas when L is too small, the difference from a Newtonian fluid becomes negligible. Because of this constraint, we chose to perform experiments at parameters corresponding to acceptable values of L, i.e. for which the estimated typical shear rate $\dot{\gamma}_s$ was above the critical shear rate of the Carreau law $\dot{\gamma}_c$ while staying of the same order of magnitude, $\dot{\gamma}_s \gtrsim \dot{\gamma}_c$. To achieve this, we operated each fluid at a chosen angle. Small $\dot{\gamma}_c$ required small angles, and we chose the following values: $\phi = 0.5°$, $\phi = 3.5°$ and $\phi = 6.5°$ for fluids 1, 2 and 3 respectively. As we can see on the rheograms of figure 2(*b*), the typical shear rates of our experiments satisfy our condition.

Our measurements followed the same protocol as described in the previous section: we measured the stability threshold for different flow rates in order to deduce the critical Reynolds number Re_c. Figure 4(*a*) shows the experimental stability thresholds for fluids 1, 2 and 3 at their inclination angles, in the (Re, f_c) plane. Again, we

Fluid	ϕ	Critical Reynolds number				
		Exp. fit	Orr–Som	Ruyer-Quil *et al.* (2012)	Ng & Mei (1994)	$\frac{5}{6}\cot\phi$
1	0.5°	38.5	35.1	34.8	34.8	95.5
2	3.5°	12.2	11.8	11.8	11.5	13.6
3	6.5°	5.7	5.79	5.7	5.45	7.3

TABLE 2. Critical Reynolds numbers found with different methods. Explanations are given in the text.

find that the neutral frequency varies as a square root expression. We can then fit (3.1) to our data and extract a critical Reynolds number. The extracted values are given in table 2 and are found to be significantly smaller than in the Newtonian case. In figure 4(*b*), we present together the experimental thresholds (symbols) and the thresholds computed from the Orr–Sommerfeld equation resolution (solid lines). The computational neutral curves fit the experimental points very well and the numerically computed critical Reynolds number is very close to the one extracted from the experiments (see table 2). The Newtonian case thresholds given by (3.2) are plotted as empty stars. The theoretical thresholds obtained by Ng & Mei (1994) with a power-law fluid and Ruyer-Quil *et al.* (2012) with a regularized power-law fluid are respectively plotted as black dots and empty diamonds.

The first outcome of these results is experimental evidence of the destabilizing effect of the shear-thinning property: in all three fluids, the critical Reynolds number is lower than in the corresponding Newtonian case, and the effect is more pronounced when the shear-thinning is important, as for fluid 1. We can also state that the critical Reynolds numbers we found, both experimentally and numerically, correspond very well to the values predicted by the theory of Ruyer-Quil *et al.* (2012) (long-wave expansion method for a power-law fluid regularized at low shear rates). They also correspond well to the values obtained with the model of Ng & Mei (1994). Finally, we want to point out that the effect of the width of the channel here is perfectly captured by the correction proposed by Georgantaki *et al.* (2011): for fluid 1, we have $Re_c/R^* = 35.3$ and for fluid 2, $Re_c/R^* = 11.7$ (for $Ka = 306$ and $Ka = 123$ respectively), which compare very well with the Orr–Sommerfeld values given in table 2. This is possibly due to the shear-thinning property, which makes the viscosity at the sides of the channel less important than for the corresponding Newtonian fluid.

Finally, figure 4(*c*) shows the wave phase speed $c = 2\pi f_c/k$, rescaled by the surface velocity U_0 (U_0 is calculated from q, ϕ and the rheology of the fluid). Again, we compare the measurements with the numerical results from the Orr–Sommerfeld formulation. The rescaled phase speed asymptotically reaches a maximum value at the stability threshold, i.e. for $k \rightarrow 0$ and $Re \rightarrow Re_c$. As expected from Millet *et al.* (2008), this maximum value is bounded within an interval of $c/U_0 \in [2, (1 + 1/n)]$, corresponding to the Newtonian and power-law limit cases of the Carreau model. It should be noted that the power-law limit is reached in the case of fluid 1 since its shear-thinning properties are much stronger.

Presented in these axes, the experimental data are noisier than in figure 4(*a,b*), mostly because the scale of variation of c/U_0 is very narrow, and therefore very sensitive to the error, but also because it cumulates uncertainties present in the f_c and k independent measurements, and on the parameters to be used in the numerical evaluation of U_0. However, the agreement between experiments and computations is still good.

The obtained overall picture is consistent with the destabilizing effect observed in figure 4(*b*): the phase speed to free-surface velocity ratio c/U_0 reaches values larger than 2 (the Newtonian value) at the threshold, and is larger when the shear-thinning is more pronounced. However, despite its ability to produce the correct critical Reynolds number, the power-law rheology model is not as good at predicting the critical wave phase speed, since the derived c/U_0 value does not reach the maximum value of $(1 + 1/n)$ for fluids 2 and 3.

5. Conclusion

In this study, stability experiments on film flows down an incline have been made for weakly to moderately shear-thinning fluids at fixed inclination angles. The results in terms of neutral curves and critical Reynolds number have been plotted in the (Re, f_c), (Re, k) and $(Re, c/U_0)$ planes, and are in good agreement with the numerical results obtained by either a full resolution of the generalized Orr–Sommerfeld equation or asymptotic expressions for the critical Reynolds number found in the literature under the long-wave expansion theory. Measurements of marginal wavelengths near the threshold remain difficult ($f < 1$ Hz; $\lambda > 20$ cm), and their uncertainties affect the results for the critical wave celerity. The probable stabilizing effect of the channel width appears to be weak in the presented experimental runs. To the best of our knowledge, this work is the first experimental measurement of the destabilizing effect induced by the shear-thinning behaviour on liquid films flowing down an inclined plane: at a given slope, the critical Reynolds number is lower and the rescaled phase speed is higher than for a Newtonian fluid.

References

ALLOUCHE, M. H., BOTTON, V., HENRY, D., MILLET, S., USHA, R. & BEN HADID, H. 2015 Experimental determination of the viscosity at very low shear rate for shear thinning fluids by electrocapillarity. *J. Non-Newtonian Fluid Mech.* **215**, 60–69.

AMAOUCHE, M., DJEMA, A. & BOURDACHE, L. 2009 A modified Shkadov's model for thin film flow of a power law fluid over an inclined surface. *C. R. Méc.* **337** (1), 48–52.

ARGYRIADI, K., SERIFI, K. & BONTOZOGLOU, V. 2004 Nonlinear dynamics of inclined films under low-frequency forcing. *Phys. Fluids* **16** (7), 2457–2468.

BENCHABANE, A. & BEKKOUR, K. 2008 Rheological properties of carboxymethyl cellulose (CMC) solutions. *Colloid Polym. Sci.* **286** (10), 1173–1180.

BENJAMIN, T. B. 1957 Wave formation in laminar flow down an inclined plane. *J. Fluid Mech.* **2** (06), 554–573.

CHAMBON, G., GHEMMOUR, A. & LAIGLE, D. 2009 Gravity-driven surges of a viscoplastic fluid: an experimental study. *J. Non-Newtonian Fluid Mech.* **158**, 54–62.

CHAMBON, G., GHEMMOUR, A. & NAAIM, M. 2014 Experimental investigation of viscoplastic free-surface flows in a steady uniform regime. *J. Fluid Mech.* **754**, 332–364.

COUSSOT, P. 1994 Steady, laminar flow of concentrated mud suspensions in open channel. *J. Hydraul. Res.* **32** (4), 535–559.

DANDAPAT, B. S. & MUKHOPADHYAY, A. 2001 Waves on a film of power-law fluid flowing down an inclined plane at moderate Reynolds number. *Fluid Dyn. Res.* **29** (3), 199–220.

DENNER, F., PRADAS, M., CHAROGIANNIS, A., MARKIDES, C. N., VAN WACHEM, B. G. M. & KALLIADASIS, S. 2016 Self-similarity of solitary waves on inertia-dominated falling liquid films. *Phys. Rev.* E **93**, 033121.

ESCUDIER, M. P., GOULDSON, I. W., PEREIRA, A. S., PINHO, F. T. & POOLE, R. J. 2001 On the reproducibility of the rheology of shear-thinning liquids. *J. Non-Newtonian Fluid Mech.* **97** (2), 99–124.

FERNÁNDEZ-NIETO, E. D., NOBLE, P. & VILA, J.-P. 2010 Shallow water equations for non-Newtonian fluids. *J. Non-Newtonian Fluid Mech.* **165** (13), 712–732.

FORTERRE, Y. & POULIQUEN, O. 2003 Long-surface-wave instability in dense granular flows. *J. Fluid Mech.* **486**, 21–50.

GEORGANTAKI, A., VATTEVILLE, J., VLACHOGIANNIS, M. & BONTOZOGLOU, V. 2011 Measurements of liquid film flow as a function of fluid properties and channel width: evidence for surface-tension-induced long-range transverse coherence. *Phys. Rev.* E **84** (2), 026325.

HUANG, X. & GARCIA, M. H. 1998 A Herschel–Bulkley model for mud flow down a slope. *J. Fluid Mech.* **374**, 305–333.

JEONG, S. W. 2010 Grain size dependent rheology on the mobility of debris flows. *Geosci. J.* **14** (4), 359–369.

JOUVET, G., PICASSO, M., RAPPAZ, J., HUSS, M. & FUNK, M. 2011 Modelling and numerical simulation of the dynamics of glaciers including local damage effects. *Math. Modelling Natural Phenom.* **6** (5), 263–280.

KALLIADASIS, S., RUYER-QUIL, C., SCHEID, B. & VELARDE, M. G. 2011 *Falling Liquid Films*. Springer.

KAPITZA, P. L. & KAPITZA, S. P. 1949 Wave flow of thin layers of viscous liquids. Part III. Experimental research of a wave flow regime. *Zh. Eksp. Teor. Fiz.* **19**, 105–120.

LIU, J., PAUL, J. D. & GOLLUB, J. P. 1993 Measurements of the primary instabilities of film flows. *J. Fluid Mech.* **250**, 69–101.

MILLET, S., BOTTON, V., ROUSSET, F. & BEN HADID, H. 2008 Wave celerity on a shear-thinning fluid film flowing down an incline. *Phys. Fluids* **20** (3), 031701.

MOISY, F., RABAUD, M. & SALSAC, K. 2009 A synthetic schlieren method for the measurement of the topography of a liquid interface. *Exp. Fluids* **46** (6), 1021–1036.

NG, C.-O. & MEI, C. C. 1994 Roll waves on a shallow layer of mud modeled as a power-law fluid. *J. Fluid Mech.* **263**, 151–183.

NOBLE, P. & VILA, J.-P. 2013 Thin power-law film flow down an inclined plane: consistent shallow-water models and stability under large-scale perturbations. *J. Fluid Mech.* **735**, 29–60.

RODD, A. B., DUNSTAN, D. E. & BOGER, D. V. 2000 Characterisation of xanthan gum solutions using dynamic light scattering and rheology. *Carbohydrate Polym.* **42** (2), 159–174.

ROUSSET, F., MILLET, S., BOTTON, V. & BEN HADID, H. 2007 Temporal stability of Carreau fluid flow down an incline. *J. Fluids Engng Trans. ASME* **129** (7), 913–920.

RUYER-QUIL, C., CHAKRABORTY, S. & DANDAPAT, B. S. 2012 Wavy regime of a power-law film flow. *J. Fluid Mech.* **692**, 220–256.

SMITH, M. K. 1990 The mechanism for the long-wave instability in thin liquid films. *J. Fluid Mech.* **217**, 469–485.

TAKAMURA, K., FISCHER, H. & MORROW, N. R. 2012 Physical properties of aqueous glycerol solutions. *J. Petrol. Sci. Engng* **9899**, 50–60.

VLACHOGIANNIS, M., SAMANDAS, A., LEONTIDIS, V. & BONTOZOGLOU, V. 2010 Effect of channel width on the primary instability of inclined film flow. *Phys. Fluids* **22** (1), 012106.

WEINSTEIN, S. J. 1990 Wave propagation in the flow of shear-thinning fluids down an incline. *AIChE J.* **36** (12), 1873–1889.

WHITHAM, G. B. 2011 *Linear and Nonlinear Waves*. Wiley.

YIH, C.-S. 1963 Stability of liquid flow down an inclined plane. *Phys. Fluids* **6** (3), 321–334.